Journal of Physics: Conference Series **692** (2016) 012003 doi:10.1088/1742-6596/692/1/012003

Disrupted bandcount doubling in an AC-DC boost PFC circuit modeled by a time varying map

Viktor Avrutin
Institute for Systems Theory and Automatic Control, University of Stuttgart, Stuttgart, Germany
E-mail: viktor.avrutin@ist.uni-stuttgart.de

Zhanybai T. Zhusubaliyev
Department of Computer Science, Southwest State University, Kursk, Russia
E-mail: zhanybai@hotmail.com

Abdelali El Aroudi
Department of Electronics, Electrical Engineering, Automatic Control, Universitat Rovira i Virgili, Tarragona, Spain
E-mail: abdelali.elaroudi@urv.cat

Danièle Fournier-Prunaret
INSA, LAAS-CNRS, Université de Toulouse, Toulouse, France
E-mail: daniele.fournier@insa-toulouse.fr

Germain Garcia
INSA, LAAS-CNRS, Université de Toulouse, Toulouse, France
E-mail: garcia@laas.fr

Erik Mosekilde
Department of Physics, The Technical University of Denmark, Lyngby, Denmark
E-mail: erik.mosekilde@fysik.dtu.dk

Abstract. Power factor correction converters are used in many applications as AC-DC power supplies aiming at maintaining a near unity power factor. Systems of this type are known to exhibit nonlinear phenomena such as sub-harmonic oscillations and chaotic regimes that cannot be described by traditional averaged models. In this paper, we derive a time varying discrete-time map modeling the behavior of a power factor correction AC-DC boost converter. This map is derived in closed-form and is able to faithfully reproduce the system behavior under realistic conditions. In the chaotic regime the map exhibits a sequence of bifurcation similar to a bandcount doubling cascade on the low frequency. However, the observed scenario appears in some sense incomplete, with some gaps in the bifurcation diagram, whose appearance to our knowledge has never been reported before. We show that these gaps are caused by high frequency oscillations.

1. Introduction

Power factor correction (PFC) circuits are power supplies that regulate an output voltage while providing a near unity power factor (PF) in the sense that the input current is proportional to the input voltage [1, 2]. Although, a variety of circuit topologies and control methods have been developed for PFC applications, the boost converter working in continuous conduction mode is commonly chosen for medium and high power (above several hundred W) applications because of its low conduction losses and reduced electromagnetic interferences filtering requirements [2].

The output voltage of a boost PFC converter (the bus voltage) must be always higher than the peak line voltage for an appropriate functioning of the system. For usual line input voltage applications (85-265 V RMS), the bus voltage is usually fixed in the range 380-400 V DC, which is achieved by an appropriate external voltage feedback compensating loop.

While the output voltage of an AC-DC PFC circuit is regulated to a desired DC value, its input is a sinusoidal time varying signal. This leads the duty cycle to vary between one and a minimum value. One of the most important tasks in the design of PFC power supplies is the implementation of the inner control loop.

While the main design criterion of maintaining a near unity PF can be achieved, in average, by using traditional control design techniques based on averaged modeling, it is well known that stability of the fundamental periodic orbit can not be achieved for all parameter values. Recently it has been shown both by numerical simulations and by experimental measurements that boost PFC converter can exhibit period doubling cascades and sub-harmonic oscillations at the line frequency as well as bubbling at the switching frequency [3, 4, 5]. This is a very undesirable behavior as it can jeopardize considerably the system performances by increasing its total harmonic distortion, as confirmed both experimentally and numerically (see for example recent publications [6, 7]). Realizing the practical importance of PFC AC-DC converters, a series of studies dealing with the nonlinear behavior in these systems have been carried out on this topic [8, 9, 10, 11].

In fact, the occurrence of bifurcations in power electronics circuits was reported in the pioneer works of Hamill and co-workers [12, 13] where the importance of studying the dynamical behavior of these systems by using iterative mappings was pointed out. Among the earliest works providing a detailed numerical and analytic investigation of bifurcations and transitions to chaos in DC-DC converters it is worth mentioning the paper by Baushev and Zhusubaliyev [14]. In this work it is shown that such systems can possess a wide range of parameters with many locally stable limit cycles with different dynamic characteristics, including regions of multistability. These cycles arise in hard transitions, and with changing parameters each of them can undergo either a finite or an infinite sequence of period-doubling bifurcations, resulting in the transition to chaos.

While in DC-DC converters, the map describing the dynamical behavior is time invariant (autonomous) [12, 13, 14], in the case DC-AC converters [15] and AC-DC converters, the map takes a time varying (non-autonomous) form [8, 16, 17]. The goal of the present paper is to present a simple time-varying map modeling the behavior of an AC-DC PFC boost converter, and to report an unusual bifurcation phenomenon which, to our knowledge, has never been reported before.

The paper is organized as follows. First, in Secs. 2 and 3 we describe the considered circuit, its model in continuous time and the discrete-time model resulting from it. Next, in Sec. 4 we show the examples of simulations in continuous and discrete time domains. Thereafter, in Sec. 5 we discuss bifurcation structures formed by chaotic attractors in the considered system. The bifurcation diagrams obtained under variation of one of the parameters appear surprisingly incomplete. We show that this is not a problem related to numerical inaccuracy but a phenomenon caused by high frequency oscillations.

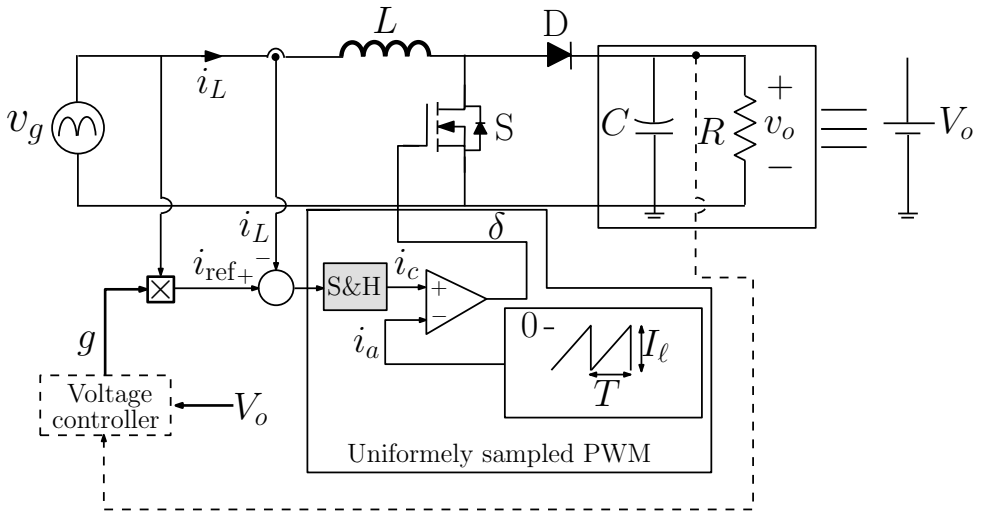

Figure 1. Boost PFC circuit designed to provide a regulated DC voltage V_o from the AC input voltage v_g while operating with a nearly uniform PF. The inductor current i_L is detected by means of a current sensor, and the error signal $i_{\text{ref}} - i_L$ is sampled at the switching frequency and processed by the current controller. The outer voltage controller (dashed structure in the figure) is not included in the model.

2. System description

Fig. 1 shows a schematic circuit diagram of a PFC boost converter designed to produce a regulated DC voltage V_o from the AC voltage source v_g while operating with a nearly uniform power factor. As shown in the figure, the inductor current i_L is measured by means of a current sensor, and the error current, represented by the difference $i_{\text{ref}} - i_L$, is sampled at the switching frequency and thereafter processed in the sample-and-hold current controller. The output of this controller i_c is connected to the non-inverting input of the comperator and a suitable saw-tooth signal i_a is applied to the inverting input of the comperator. This is used to control the operation of the switch S. This operation is arranged in such a way that the switch S switches ON at the beginning of each switching period cycle and switches OFF whenever the ramp voltage i_a exceeds the control signal i_c. The diode D is activated in a manner complementary to the activation of S. The capacitor with capacitance C and the resistor with resistance R represent a smoothing filter that provides a smooth autonomous component to the dynamics of the system.

In order to regulate the output voltage v_o to a desired value V_o an outer voltage control loop is used (the structure shown dashed in Fig. 1). The crossover frequency of this controller must be of the order of some Hz for the ripple associated with the voltage feedback to be small, and the harmonic distortion of the line current acceptable.

During steady state operation, the converter is designed to operate with periodic wave forms for the various state variables. The system is subjected to two external periodicities: the switching period T and the line period $T_l \gg T$. To ensure that the average value of the inductor current is in phase with the input voltage, the reference current i_{ref} is given by the input voltage $v_g(t)$ multiplied by a suitable conductance g:

$$i_{\text{ref}}(t) = g\, v_g(t). \tag{1}$$

Here the conductance g is provided by the output of the external voltage controller. The signal

$$v_g(t) = V_g |\sin(\omega t)| \tag{2}$$

is the rectified sinusoidal source voltage with the constant amplitude V_g and the angular frequency $\omega = 2\pi/T_l$. In practice, the value of g is the conductance given by an external loop controller regulating the output voltage v_o and which is related to the rated power of the converter. However, in most applications this conductance as well as the output voltage can be considered as constant ($g = G$ and $v_o = V_o$). Indeed, in practice the output voltage is regulated to constant DC value by means of an appropriate controller. Since the small ripple in this output voltage has no effect on the phenomena reported in this study, the ripple of this voltage and its controller can be neglected. This approximation will also allow us to obtain the time varying map in closed form. Therefore, in the following, to simplify the analysis we shall ignore the outer loop. Hence, the inductor current represents the only state variable of our model.

Among many control algorithms that can be used for performing the PFC operation, in this work we choose a simple control strategy in which the value of the duty cycle $d(nT)$ is programmed digitally according the following law

$$d(nT) = d_n = \frac{1}{I_\ell}(-i_{\text{ref}}(nT) + i_L(nT) + I_\ell) \tag{3}$$

where I_ℓ as defined in Fig. 1 is the amplitude of the ramp signal. It should be noted that because the duty cycle is defined cycle by cycle, its expression in (3) has a physical meaning only in the interval $(0, 1)$. If that expression gives values outside this interval, the duty cycle will be saturated to 0 or 1.

The behavior of the considered converter is described by the differential equation

$$\frac{\mathrm{d}x}{\mathrm{d}t} = \begin{cases} \dfrac{v_g(t)}{L} & \text{if } \delta(t) = 1 \\ \dfrac{v_g(t)}{L} - \dfrac{V_o}{L} & \text{if } \delta(t) = 0 \end{cases} \tag{4}$$

where $x = i_L$, while $\dfrac{v_g(t)}{L}$ and $\dfrac{V_o - v_g(t)}{L}$ are the time varying rising and falling slopes of the inductor current within a switching cycle. In Eq. (4) $\delta(t)$ is the driving binary signal with the duty cycle $d(t)$ applied to the switch which is generated by $T-$periodic PWM process, V_o is the output voltage.

3. Time varying map

Let us suppose that t is such that $\sin(\omega t) > 0$ and therefore $|\sin(\omega t)| = \sin(\omega t)$. During the ON phase ($\delta(t) = 1$), i.e., within the interval $nT < t < t_n$, $t_n = (n + d_n)T$, Eq. (4) has the form

$$\frac{\mathrm{d}x}{\mathrm{d}t} = \frac{V_g}{L}\sin(\omega t), \quad x(nT) = x_n, \tag{5}$$

with the solution

$$x(t) = x_n - \frac{V_g}{L\omega}\left[\cos(\omega t) - \cos(\omega nT)\right], \tag{6}$$

or, at the switching time $t = t_n$,

$$x(t_n) = x_n - \frac{V_g}{L\omega}\left[\cos(\omega t_n) - \cos(\omega nT)\right]. \tag{7}$$

At the time $t = t_n$, the converter switches to the phase OFF, and in the subsequent time interval $t_n \leqslant t \leqslant (n + 1)T$, Eq. (4) takes the form

$$\frac{\mathrm{d}x}{\mathrm{d}t} = \frac{V_g}{L}\sin(\omega t) - \frac{V_o}{L}, \tag{8}$$

with the solution

$$x(t) = x(t_n) - \frac{V_o}{L}(t - t_n) - \frac{V_g}{L\omega}[\cos(\omega t) - \cos(\omega t_n)]. \tag{9}$$

Hence, for $t = (n+1)T$ we obtain

$$x_{n+1} = x(t_n) - \frac{V_o}{L}(1 - d_n)T - \frac{V_g}{L\omega}[\cos(\omega(n+1)T) - \cos(\omega t_n)], \tag{10}$$

with $x_{n+1} = x((n+1)T)$. Substituting the expression (7) into (10), we obtain the map for the first half line cycle, i.e., for $\omega nT \leqslant \pi$:

$$x_{n+1} = x_n - \frac{V_o}{L}(1 - d_n)T - \frac{V_g}{L\omega}\big[\cos(\omega(n+1)T) - \cos(\omega nT)\big]. \tag{11}$$

For the remaining half cycle the calculations can be done similarly by inverting the sign of the sine function. In this way we obtain

$$x_{n+1} = \begin{cases} x_n - \dfrac{V_o}{L} z_n T - \dfrac{V_g}{L\omega} \cdot [\cos(\omega(n+1)T) - \cos(\omega nT)] & \text{if } \sin(\omega nT) \geqslant 0 \\ x_n - \dfrac{V_o}{L} z_n T + \dfrac{V_g}{L\omega} \cdot [\cos(\omega(n+1)T) - \cos(\omega nT)] & \text{if } \sin(\omega nT) < 0 \end{cases} \tag{12a}$$

where

$$z_n = 1 - d_n = \begin{cases} 0 & \text{if } x_n < r_n, \\ \dfrac{r_n - x_n}{I_\ell} & \text{if } r_n \leqslant x_n \leqslant r_n + I_\ell, \\ 1 & \text{if } x_n > r_n + I_\ell \end{cases} \tag{12b}$$

and $r_n = i_{\text{ref}}(nT) = gV_g \sin(\omega nT)$.

Let the ratio between the line period and the switching period be $m = T_l/T$. In practice the line period is much higher than the switching period and therefore m takes high values. For instance, the set of frequency values used in this paper leads to $m = 1000$. Under these conditions, Eq. (12a) can be rewritten as

$$x_{n+1} = \begin{cases} x_n - \dfrac{V_o}{L} z_n T - \dfrac{V_g}{L\omega}\left[\cos\left(2\pi\dfrac{n+1}{m}\right) - \cos\left(2\pi\dfrac{n}{m}\right)\right] & \text{if } \sin\left(2\pi\dfrac{n}{m}\right) \geqslant 0 \\ x_n - \dfrac{V_o}{L} z_n T + \dfrac{V_g}{L\omega}\left[\cos\left(2\pi\dfrac{n+1}{m}\right) - \cos\left(2\pi\dfrac{n}{m}\right)\right] & \text{if } \sin\left(2\pi\dfrac{n}{m}\right) < 0 \end{cases} \tag{13}$$

Eq. (13) defines a non-autonomous 1D map which can easily be transformed into an autonomous 2D map by extending the state space and considering the discrete time n as a new state variable. As sine and cosine functions in Eq. (13) are m-periodic, this new variable can be considered modulo m:

$$x_{n+1} = \begin{cases} x_n - \dfrac{V_o}{L} z_n T - \dfrac{V_g}{L\omega}\left[\cos\left(2\pi\dfrac{k_n+1}{m}\right) - \cos\left(2\pi\dfrac{k_n}{m}\right)\right] & \text{if } \sin\left(2\pi\dfrac{k_n}{m}\right) \geqslant 0 \\ x_n - \dfrac{V_o}{L} z_n T + \dfrac{V_g}{L\omega}\left[\cos\left(2\pi\dfrac{k_n+1}{m}\right) - \cos\left(2\pi\dfrac{k_n}{m}\right)\right] & \text{if } \sin\left(2\pi\dfrac{k_n}{m}\right) < 0 \end{cases} \tag{14a}$$

$$k_{n+1} = (k_n + 1) \bmod m, \quad k_0 = 0 \tag{14b}$$

Moreover, when m is an even number, the map (14a) can be further simplified by restricting the variable k to the interval $\mathbb{K} = [0, m/2 - 1]$. Indeed, since $\forall\phi : \cos(\phi) = -\cos(\phi - \pi)$, the

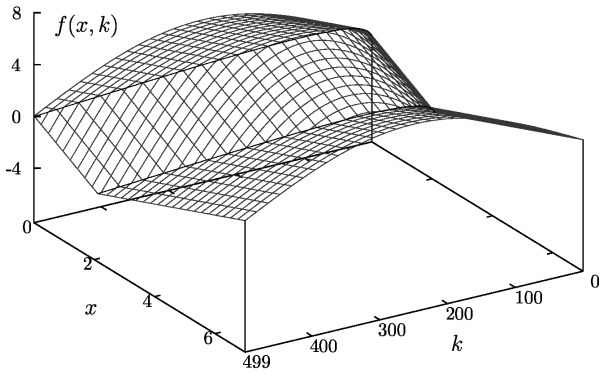

Figure 2. A typical shape of the function f. As one can see, for each fixed k the function $f(x, k^*)$ as a function of x is bimodal. One period of $f(x, k)$ with respect to k is shown. Parameters: $I_\ell = 2.1$A, $m = 1000$.

expressions for $\sin(2\pi k_n/m) \geqslant 0$ and $\sin(2\pi k_n/m) < 0$ can be unified. This leads to the final expression of our model

$$x_{n+1} = f(x_n, k_n) = x_n + \frac{V_g}{L\omega}\cos\left(2\pi\frac{k_n}{m}\right) - \frac{V_g}{L\omega}\cos\left(2\pi\frac{k_n+1}{m}\right) - \frac{V_o}{L}z_n T, \tag{15a}$$

$$k_{n+1} = h(k_n) = (k_n + 1) \bmod \frac{m}{2}, \quad k_0 = 0 \tag{15b}$$

where z_n is given by Eq. (12b) and r_n can be rewritten as follows:

$$r_n = i_{\text{ref}}(k_n) = gV_g \sin\left(2\pi\frac{k_n}{m}\right). \tag{15c}$$

Note the variable k corresponds to the discrete time restricted to the interval $\mathbb{K}$ and takes integer values

$$k_n = n \bmod \frac{m}{2}. \tag{16}$$

After extending the state space by considering the discrete time k_n as a new state variable, the model in (15) represents an autonomous triangular map where f in Eq.(15a) depends both on x and k, while h in Eq.(15b) depends on k only. Because of the possible saturation of the duty cycle (see Eq.(12b)), the phase space $\mathbb{R}_+ \times \mathbb{K}$ of map (15) consists of three partitions separated by the following two borders

$$s^- = \{(x, k) \mid x = r_k\} \tag{17a}$$

$$s^+ = \{(x, k) \mid x = r_k + I_\ell\}. \tag{17b}$$

On the outer partitions the function f is linear and increasing with respect to x, while on the middle partition it is non-linear and decreasing, so that for each fixed k, f as a function of x is bimodal, as illustrated in Fig. 2. It is worth noticing that this kind of maps results from the modeling of several other classes of power-converters (see [17] for an example).

4. Numerical simulations

Let us fix the following set of parameter values, determined by physical parameters of the considered circuit: $g = 0.01$ S, $V_g = 220\sqrt{2}$ V, $\omega = 2\pi \cdot 50$ rad/s, $V_o = 380$ V, $L = 150$ μH,

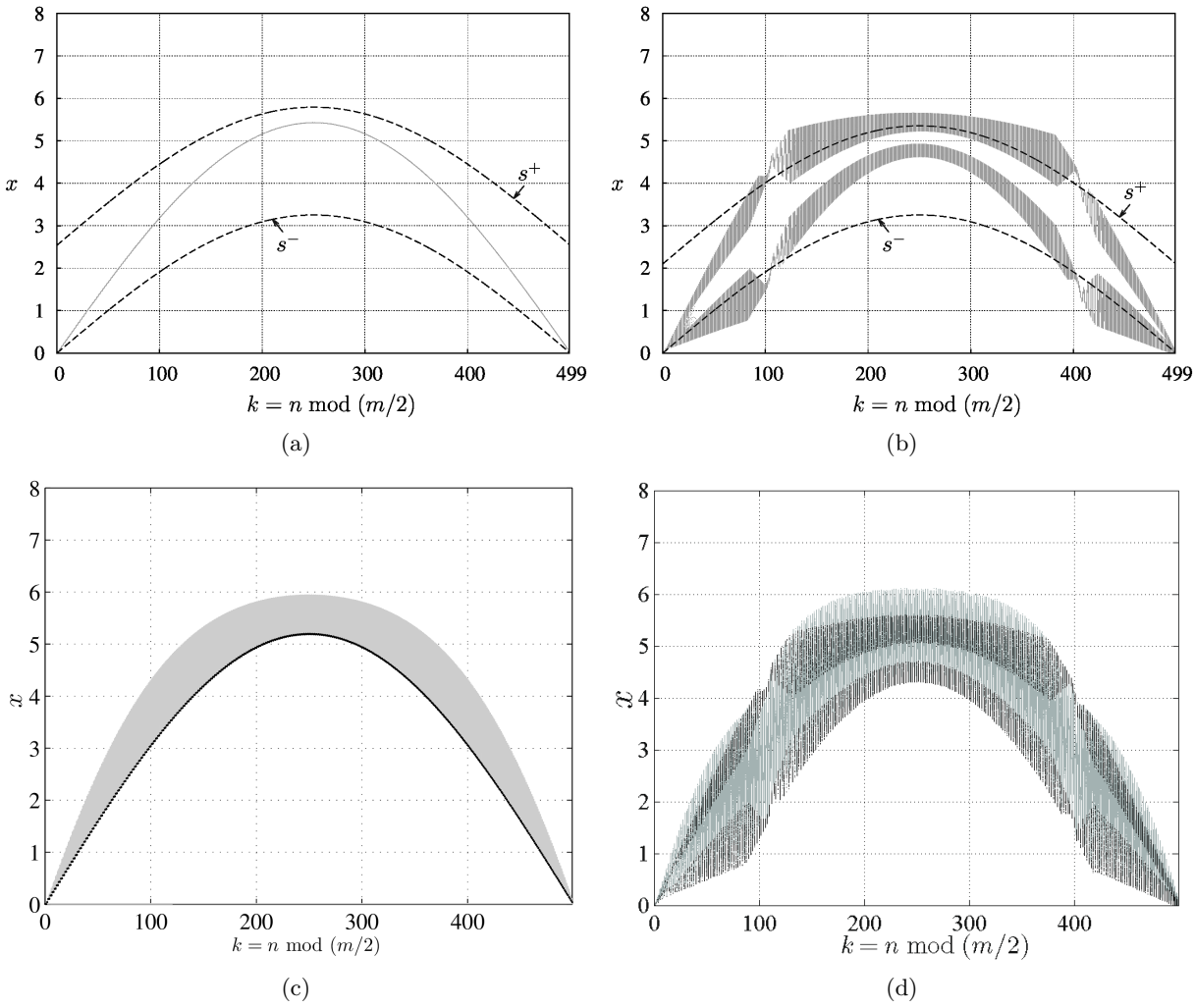

Figure 3. (a) A stable cycle and (b) a two-band chaotic attractor of map (15). Additionally, in (a) and (b) the boundaries $s^{\pm}$ are shown. In (c) and (d) the time-series obtained in continuous-time simulations at the same parameter values as in (a) and (b) are shown, dots indicate the values obtained by sampling the time series with the switching frequency. Parameters: (a), (c): $I_\ell = 2.54$A, (b), (d): $I_\ell = 2.1$A.

$T = 2\ \mu$s, and explore the possible dynamical behaviors that the system exhibits under variation of the parameter I_ℓ (recall that this parameter determines the amplitude of the ramp function). Fig. 3 shows the system behavior in the state space (k_n, x_n) for two different values of I_ℓ. In Fig. 3(a) an example for periodic dynamics of map (15) is presented, corresponding to the desired operational regime of the circuit. In this case the controller is able to impose a near unity PF for the system since, in average, the inductor current is proportional to the rectified sinusoidal input voltage without any irregular oscillation. However, this is not the case for Fig. 3(b) which shows a chaotic attractor of map (15).

For comparison, the system is also simulated using a circuit-based continuous-time switched model implemented in PSIM [18]. The resulting wave forms are shown in Fig. 3(c)-(d). As one can see, the results of continuous-time and discrete-time simulations are in a good agreement.

5. Chaotic attractors

As inspection of the figure shows, the chaotic attractor in Fig. 4(a) is located inside the absorbing area confined by the curves defined by the images of the borders:

$$c^{0,\pm} = \left\{(x,k) \mid x = f\left(k^{(-1)}, s^{\pm}_{k^{(-1)}}\right)\right\} \tag{18a}$$

$$c^{1,\pm} = \left\{(x,k) \mid x = f\left(k^{(-1)}, f\left(k^{(-2)}, s^{\pm}_{k^{(-2)}}\right)\right)\right\} \tag{18b}$$

where

$$k^{(i)} = (k+i) \bmod m/2 \tag{18c}$$

One immediately observes that for each fixed $k = \tilde{k}$ the attractor consists of two bands, which are mapped by f on the corresponding two bands at the next value $k = \tilde{k}^{(1)}$. It is worth noticing that the size and the oscillations of the bands depends strongly on k. For example, for k close to $m/4$ the bands are broad and do not oscillate. By contrast, there are two intervals for k close to $m/8$ and $3m/8$ in which the bands suddenly decrease in size and high frequency oscillations appear.

The high frequency oscillations mentioned above lead to phenomena which may be misleading on the large scale. For example, for $k > 120$ the chaotic attractor shown in Fig. 4(b) seems to consist of four bands. However, it is clearly visible in the magnification that for each value of k the attractor has only one band, i.e., it is a one-band attractor. Remarkably, with increasing k the bands are cyclically rotating taking one of four possible positions, which leads to the large-scale structure misleadingly resembling a four-band attractor.

Numerical simulations suggest that by decreasing the parameter I_ℓ we observe a sequence of bifurcations forming a cascade which is similar to a bandcount doubling cascade well known for piecewise smooth 1D maps [19]. Recall that in continuous maps such a cascade is formed by merging bifurcations [20] and shows a sequence of chaotic attractors with $\mathcal{K} = p \cdot 2^i$ bands, $i = 0, 1, 2, \ldots$, accumulating to a parameter value at which a p-cycle changes its stability [19]. In the 2D map (15), a similar scenario can be observed under variation of I_ℓ, and also the Lyapunov exponents (see Fig. 5(d)) show the structure typical for such transitions to chaos. Note that in order to avoid difficulties related to the discrete-valued variable k, the Lyapunov exponents are calculated not for the map (15), but for the $(m/2)$th iterate $f^{m/2}$ of its first component f (see Eq. (15a)). It can easily be shown that $f^{m/2}$ represents a 1D stroboscopic map of map (15) and reflects its dynamics completely.

In addition, an unusual phenomenon can be observed in Fig. 5, namely that the bifurcations diagrams calculated at different fixed values of k appear incomplete and exhibit remarkable gaps. The location of these gaps depends on k and at the present, the observed phenomenon is far from being completely investigated. It can already be said that it results from two different mechanisms:

(i) As usual for bandcount doubling cascades in 1D maps, there are nested absorbing areas in the state space, and the number of their connected components determines the position in the bandcount doubling cascade. For example, at the parameter value corresponding to Fig. 4(a) there exists an overall absorbing area with one connected component confined by the first two images of the borders ($c^{i,\pm}$, $i = 0, 1$; as described above). Inside this absorbing area there exists a nested absorbing area with two connected components, confined by the first four images of the borders ($c^{i,\pm}$; $i = 0, 1, 2, 3$). This phenomenon is independent on k and explains the overall shape of the observed bifurcation diagrams.

(ii) In addition to the described phenomenon, there are oscillations whose appearance depends on k. As a consequence, at some values of k the bands of chaotic attractors fill the connected

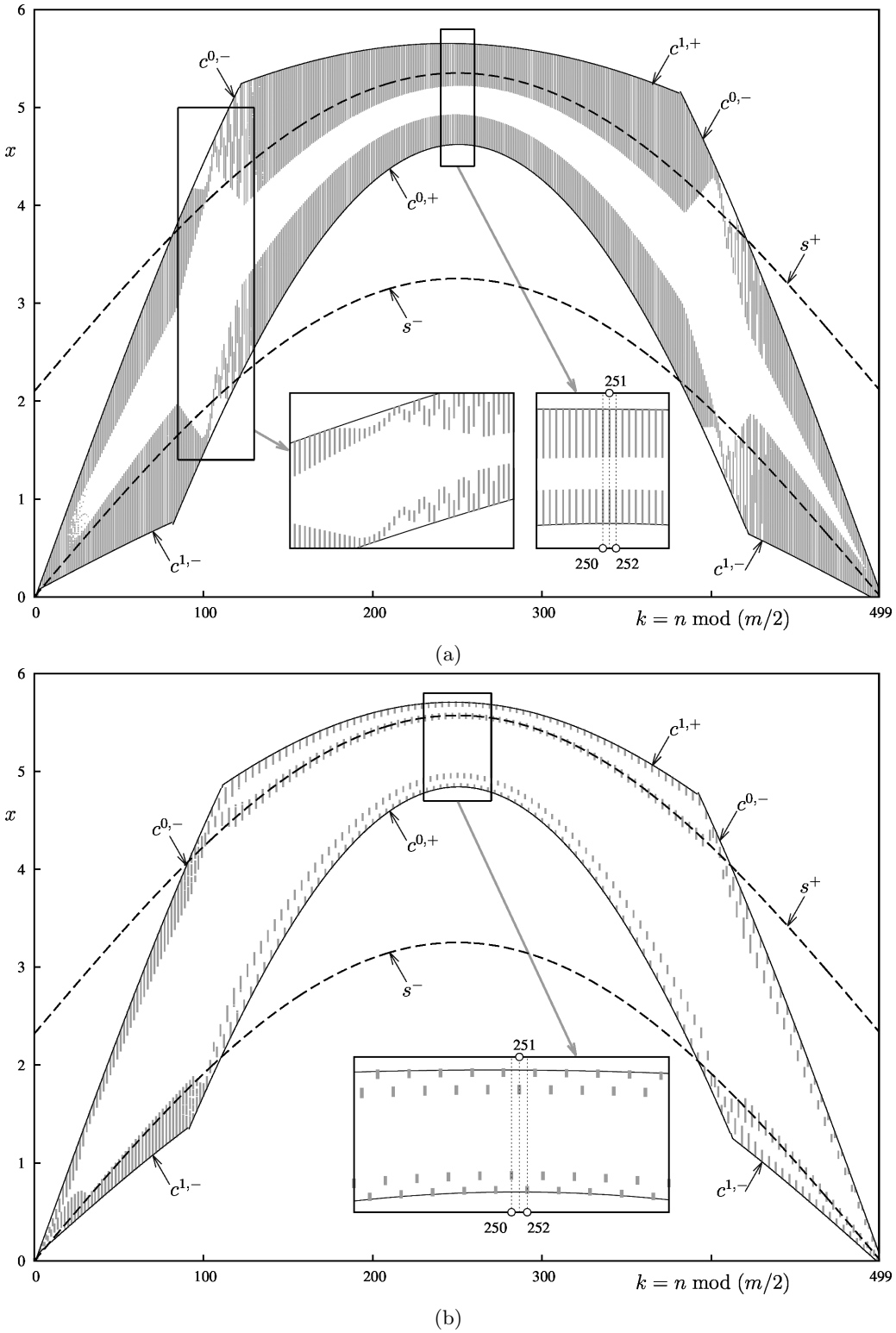

Figure 4. Chaotic attractors of map (15): (a) a two-band attractor; (b) a one-band attractor. Additionally, the borders $s^{\pm}$ and their images of rank 1 and 2 are shown. The values $k = 250$, 251, 252 corresponding to the bifurcation diagrams shown in Fig. 5(a), (b) and (c), respectively, are marked in the magnifications. Parameters: (a) $I_\ell = 2.1$A, (b) $I_\ell = 2.32$A. In Fig. 5 these parameter values are marked with B and C, respectively

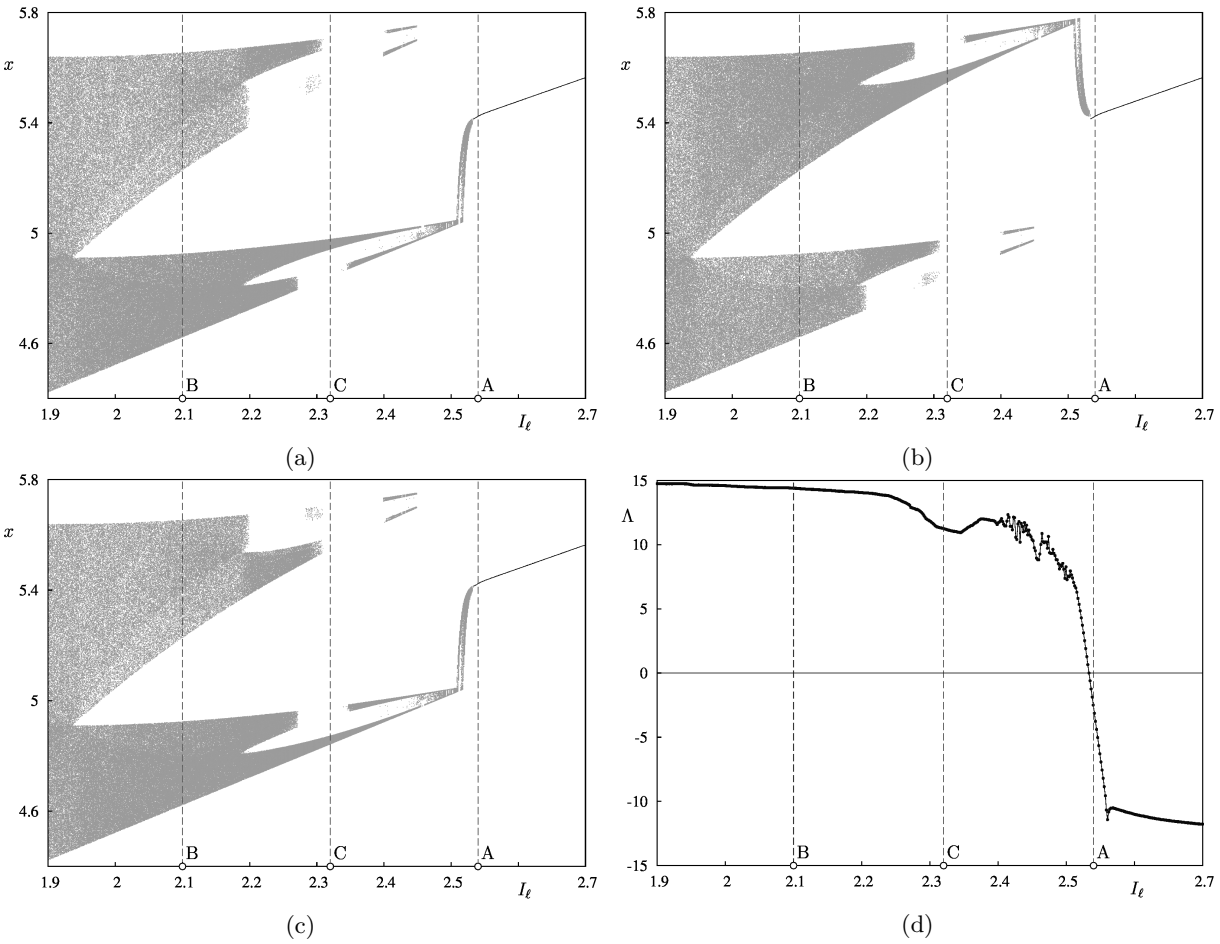

Figure 5. Bifurcation diagrams obtained under variation of I_ℓ at (a) $k = 250$, (b) $k = 251$ and (c) $k = 252$. The attractor at the parameter value marked with A is shown in Fig. 3(a), at the value marked with B in Figs. 3(b) and 4(a), and at the value marked with C in Fig. 4(b). In (d) the Lyapunov exponent Λ is shown, calculated using the $(m/2)$th iterate $f^{m/2}$.

components of the absorbing areas mentioned above, while at the others they do not. This can be observed for example in the magnifications of the attractor shown in Fig. 4(a). In the right magnification (which shows the interval $245 \leqslant k \leqslant 265$) the boundaries of the chaotic attractor are given by the first four images $c^{i,+}$; $i = 0, 1, 2, 3$ of the border. By contrast, in the left magnification (showing the interval $85 \leqslant k \leqslant 130$) the first four images of the borders are not sufficient to describe the boundaries. Similarly, for each k the band of the one-band attractor shown in Fig. 4(b) fills one of four intervals. All together, these four intervals fit to the bandcount doubling structure mentioned above. However, as at each fixed k only one of them is filled, causing the resulting bifurcation diagram calculated at this particular value of k to appear incomplete. For example, at $k = 250$ (this value is labeled in the magnification in Fig. 4(b)) the second interval from below is filled, so that only this band is present in the bifurcation diagram calculated at this value of k (see Fig. 5(a) and the parameter value labeled by the letter C). For the next values of k, i.e., for $k = 251$ and $k = 252$, the third and the first intervals from below are filled, respectively. This explains the differences between Figs. 5(a), 5(b) and 5(c).

The mechanism described above explains the appearance of gaps on the bifurcation diagrams shown Fig. 5 and shows that they are not related to numerical inaccuracies. As a next step,

remaining for a future work, it is necessary to investigate the bifurcations leading the number of bands to change and to find the regularities in their occurrence.

6. Conclusions

Over the last couple of decades, active PFC circuits have become common in power supply systems in a broad range of applications such as telecommunications, computing equipment and micro-grids among others. The advantage of using active circuits is the higher efficiency and the better power quality than in passive circuits. The penalty is the added complexity that results from using switching devices working in nonlinear regime. This may cause the basic periodic operating modes to disappear through nonsmooth bifurcation phenomena, and may also introduce new oscillatory regimes in the system, leading to poor performances in terms of the power quality. In this paper an investigation of the dynamics of an AC-DC boost converter working as a PFC circuit was performed by using a nonlinear piecewise smooth time varying map. The results obtained from this map were validated by a circuit-based switched model. Nonsmooth bubbling phenomena have been observed. Numerical simulations show that when some parameter values change a sequence of bifurcations forming a cascade which is similar to a bandcount doubling cascade is observed. However, in the considered case the bifurcation scenario is more complicated, as it results from a mixture of time-independent appearance and disappearance of nested absorbing areas on one side and time-dependent bubbling-related phenomena. To our knowledge similar effects have never been reported before.

Acknowledgement

The work of V. Avrutin was partially supported by the German Research Foundation within the scope of the project *"Organizing centers in discontinuous dynamical systems: bifurcations of higher codimension in theory and applications"*.

References

[1] O. Garcia, J. A. Cobos, R. Prieto, P. Alou, J. Uceda, "Single phase power factor correction: a survey", *IEEE Trans. on Power Electronics,* vol. 18, no. 3, pp. 749-755, 2003.

[2] J. Sebastian, D. G. Lamar, M. M. Hernando, A. Rodriguez-Alonso, and A. Fernandez, "Steady-state analysis and modeling of power factor correctors with appreciable voltage ripple in the output-voltage feedback loop to achieve fast transient response", *IEEE Trans. on Power Electronics,* vol. 24, no. 11, pp. 2555-2566, 2009.

[3] H. H. C. Iu, Y. Zhou, and C. K. Tse, "Fast-scale instability in a boost PFC converter under average current control", *Int. J. of Circuit Theory and Applications,* vol. 31, pp. 611-624, 2003.

[4] M. Orabi and T. Ninomiya, "Nonlinear dynamics of power-factor-correction converter", *IEEE Trans. on Power Electronics,* vol. 50, no. 6, pp. 1116-1125, 2009.

[5] S. C. Wong, C. K. Tse, M. Orabi and T. Ninomiya, "The method of double averaging: an approach for modeling powerfactor-correction switching converters", *IEEE Trans. on Circuits and Systems I,* vol. 53, no. 2, pp. 454-462, 2006.

[6] W. Lu, Sh. Lang, L. Zhou, H. H.-Ch. Iu and T. Fernando, "Improvement of Stability and Power Factor in PCM Controlled Boost PFC Converter With Hybrid Dynamic Compensation", *IEEE Trans. on Circuits and Systems I,* vol. 62, no. 1, pp. 320-328, 2015.

[7] W. Cheng, J. Song, H. Li and Y. Guo, "Time-Varying Compensation for Peak Current-Controlled PFC Boost Converter", *IEEE Trans. on Power Electronics,* vol. 30, no. 6, pp. 3431-3437, 2015.

[8] A. El Aroudi, M. Orabi and L. Martinez-Salamero, "A representative discrete-time model for uncovering slow and fast scale instabilities in boost power factor correction AC-DC pre-regulators", *Int. J. of Bifurcation and Chaos,* vol. 18, no. 10, pp. 3073-3092, 2008.

[9] G. Chu, C. K. Tse, and S-C Wong, "Line-frequency instability of PFC power supplies", *IEEE Trans. on Power Electronics,* vol. 24, no. 2, pp. 469-482, 2009.

[10] A. El Aroudi and M. Orabi, "Stabilizing technique for AC/DC boost PFC converter based on time delay feedback",*IEEE Trans. on Circuits and Systems II: Express Briefs,* vol. 57, no. 1, pp. 56-60, 2010.

[11] A. El Aroudi and M. Orabi, "Dynamics of PFC power converters subject to time-delayed feedback control", *Int. J. of Circuit Theory and Applications,* vol. 40, no. 1, pp. 15-35, 2012.
[12] J. H. B. Deane and D. C. Hamill, "Instability, subharmonics, and chaos in power electronic systems", *IEEE Trans. on Power Electronics,* vol. 5, no. 2, pp. 260-268, Jul. 1990.
[13] D. C. Hamill, J. H. B. Deane, and D. Jefferies, "Modeling of chaotic DC-DC converters by iterated nonlinear mappings", *IEEE Trans. on Power Electronics,* vol. 7, no. 1, pp. 25-36, 1992.
[14] V. S. Baushev and Z. T. Zhusubaliyev, "Indeterminable states of a voltage regulator with pulse-width control", *Electrical Technology* vol.3, pp. 85-88, 1992.
[15] B. Robert and C. Robert, "Border Collision Bifurcations in a one-dimensional piecewise smooth map for a PWM current-programmed H-bridge inverter", *Int. J. of Control*, vol. 7, no. 16, pp. 1356-1367, 2002.
[16] Z. T. Zhusubaliyev, E.Mosekilde, A. I Andriyanov and V. V. Shein V.V, "Phase synchronized quasiperiodicity in power electronic inverter systems", *Physica D: Nonlinear Phenomena,* vol. 268, pp. 14-24, 2014.
[17] V. Avrutin, E.Mosekilde, Z.T. Zhusubaliyev and L. Gardini, "Onset of chaos in a single-phase power electronic inverter", *Chaos: An Interdisciplinary J. of Nonlinear Science,* vol. 25, pp. 043114, 2015.
[18] `http://www.powersimtech.com/`
[19] V. Avrutin and I. Sushko, "A gallery of bifurcation scenarios in piecewise smooth 1D maps", *Global Analysis of Dynamic Models in Economics, Finance and the Social Sciences*, Springer, pp. 369-395, 2015.
[20] V. Avrutin, L. Gardini, M. Schanz and I. Sushko, "Bifurcations of chaotic attractors in one-dimensional maps", *Int. J. of Bifurcation and Chaos,* vol. 24, no. 8, pp. 1440012, 2014.